Dimensionality-driven in-plane antiferromagnetism in two-dimensional $SrRuO_3$

Mo Zhu,[1,*] Zhangzhang Cui,[1,2,*,†] Yingying Zhang,[3,‡] Zheling Shan,[1] Weiwei Li,[1] Qingyou Lu,[1,2,4] Zhengcao Li,[3] and Yalin Lu[1,2,§]

[1]*Hefei National Research Center for Physical Sciences at the Microscale, and Department of Materials Science and Engineering, University of Science and Technology of China, Hefei, Anhui 230026, China*

[2]*Anhui Laboratory of Advanced Photon Science and Technology, University of Science and Technology of China, Hefei, Anhui 230026, China*

[3]*State Key Laboratory for New Ceramics and Fine Processing, Key Laboratory of Advanced Materials of Ministry of Education, School of Materials Science and Engineering, Tsinghua University, Beijing 100084, China*

[4]*Anhui Key Laboratory of Condensed Matter Physics at Extreme Conditions, High Magnetic Field Laboratory and Hefei Science Center, Chinese Academy of Sciences, Hefei, 230031, China*

(Received 27 April 2022; revised 28 December 2022; accepted 2 February 2023; published 14 February 2023)

Control of dimensionality is a powerful tool to unlock hidden electronic and magnetic phases. In particular, reduced dimensionality in strongly correlated oxides leads to an intriguing "dead-layer" behavior that a transition from (ferromagnetic) metal to (antiferromagnetic) insulator occurs as the thickness approaches the two-dimensional limit. However, the origin of such transition has been a subject of debate that both the intrinsic dimensionality effect and the extrinsic disorder effect are proposed to be the driving force. Here, we reveal a transition from ferromagnetic metal with perpendicular magnetic anisotropy to antiferromagnetic insulator with in-plane magnetic anisotropy in $SrRuO_3$ epitaxial films down to the monolayer limit. Experimentally, we demonstrate that $SrRuO_3$ films below 3 unit cells become magnetic insulators and the spin easy axis changes to the in-plane ⟨110⟩ directions. First-principles calculations reveal that the interplay of the orbital-selective quantum confinement on Ru 4*d* orbitals and the oxygen octahedral rotation drives the ultrathin films from ferromagnetic metal to antiferromagnetic insulator, reorienting Ru spins from the perpendicular to the ⟨110⟩ directions. Our findings demonstrate how reduced dimensionality can tailor the magnetic state and provide significant advances in one of the debated topics in complex oxide heterostructures that dimensionality effect alone can be the driving force of dead-layer phenomenon in two-dimensional systems.

DOI: 10.1103/PhysRevB.107.064418

I. INTRODUCTION

Reduction in dimensionality has been a powerful tool for creating emergent quantum phenomena, examples including two-dimensional (2D) magnetism [1–3], 2D electron gas [4–6], interface superconductivity [7,8], interfacial magnetism [9–13], etc. However, an obstacle in reducing the dimensionality towards the 2D limit is the occurrence of the dead-layer behavior. Below a critical thickness, the ferromagnetism and metallicity are suppressed and a nonmagnetic or antiferromagnetic (AFM) insulating state emerges. This phenomenon is commonly seen in many strongly correlated oxides including $LaNiO_3$ [14], $La_{1-x}Sr_xMnO_3$ [15], $SrRuO_3$ [16,17], $SrVO_3$ [18,19], $SrIrO_3$ [20], etc. Though extensive research efforts have been devoted, the origin of such metal-insulator transition (MIT) in the ultrathin limit has been a subject of strong debate. Generally, the intrinsic dimensionality effect including quantum confinement [21–23], charge/spin ordering [24], substrate-induced strain/coupling of oxygen octahedra [25,26], etc., and the extrinsic disorder effect such as cation off stoichiometry [19,27,28] or interface intermixing [29], are proposed to be the driving force of the thickness-dependent MIT. Though the MIT in several oxides was reported to be driven by the dimensionality effect, such as $SrVO_3$ [23], there are also disagreements due to the challenge to exclude the extrinsic effect [19].

Thick $SrRuO_3$ (SRO) epitaxial films are ferromagnetic (FM) metal with uniaxial magnetic anisotropy [30]. Extensive experimental works demonstrate that a transition to non-FM insulating state occurs in SRO films below the thickness of 2 [31], 3 [32,33], or 4 [34,35] unit cells (u.c.). There are a few reports showing the signature of metallic phase in SRO films below 2 u.c., only when the films are sandwiched between other oxide layers [36–38]. The controversy regarding the critical thickness of the MIT could be attributed to the unavoidable structural/chemical disorders and thickness nonuniformity in fabricating complex oxide films using a layer-by-layer growth technique. On the other hand, it is quite challenging to experimentally characterize the magnetic properties of ultrathin films. Xia *et al.* report a very weak exchange bias in 2- and 3-u.c. SRO films by measuring the polar Kerr effect, implying an AFM phase in these films [32], while the details of the AFM phase, including the transition temperature, the spin easy axis, etc., are unknown.

*These authors contributed equally to this work.
†zzcui@ustc.edu.cn
‡zyy2023@tsinghua.edu.cn
§yllu@ustc.edu.cn

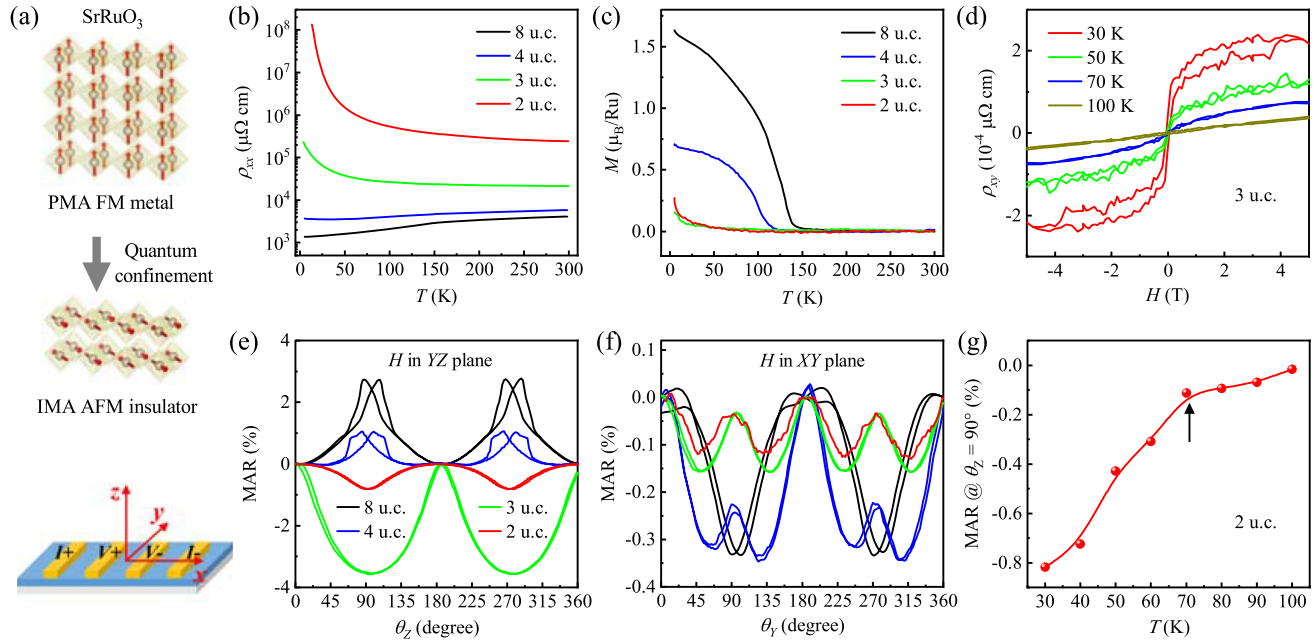

FIG. 1. Magnetic and transport measurements of ultrathin SRO films. (a) Schematic illustrations of the MAR measurement geometry (bottom panel) and the thickness-dependent magnetic phase transition from FM with perpendicular magnetic anisotropy to AFM with in-plane magnetic anisotropy (top panel). Temperature-dependent (b) resistivities and (c) out-of-plane magnetizations of 8-, 4-, 3-, and 2-u.c. SRO films. The magnetizations were recorded at 0.05 T after field cooling at 0.5 T. (d) Hall resistivitity of 3-u.c. SRO film measured at $T = 30$, 50, 70, and 100 K. Magnetic-field angle-dependent resistivity measurement of SRO films with the field sweeping in the (e) *YZ* and (f) *XY* planes. MARs of 8-, 4-, and 3-u.c. films were recorded with $H = 5$ T at $T = 5$ K. As the resistivity of 2-u.c. film below 20 K is over the measurement limit, the MAR was measured with $H = 9$ T at $T = 30$ K in panel (e) and $T = 20$ K in panel (f). For clarity, MARs of 3-u.c. film are divided by a factor of 10. θ_Z is the angle between the field and z axis, and θ_Y is the angle between the field and y axis. (g) Temperature-dependent MAR value at $\theta_Z = 90^\circ$ of 2-u.c. SRO film.

Theoretically, first-principles calculations utilizing distinct parameters give inconsistent ground states of SRO films in the 2D limit, including nonmagnetic metallic [31,36], FM metallic [29,39], and AFM insulating states [40–44]. Particularly, oxygen octahedral rotation (OOR) and on-site Coulomb repulsion (U) play essential roles in determining the ground state. In general, due to the coexistence of intrinsic dimensionality effect and extrinsic structural/chemical disorders, as well as the inconsistency in theoretical calculations, it is difficult to reach a consensus on the origin of thickness-dependent MIT in SRO films.

In this work, we demonstrate a dimensionality-driven magnetic phase transition from FM metal with perpendicular magnetic anisotropy (PMA) to AFM insulator with in-plane magnetic anisotropy (IMA) [as schematically shown in Fig. 1(a), top panel] by fabricating ultrathin SRO films with thickness down to the monolayer limit. Transport and magnetic characterizations show that the films remain FM metallic down to 4 u.c., but the 3- and 2-u.c. films become AFM insulating with ⟨110⟩ magnetic easy axes. Our density-functional theory (DFT) calculations further elucidate these experimental findings and reveal that the orbital-selective quantum confinement effect (QCE) and out-of-plane OOR lead to the reconstruction of Ru 4*d* orbitals, resulting in an AFM insulating state and reorienting Ru magnetic moment. Furthermore, we exclude the possible role of structural defects in driving the magnetic phase transition by controlling the oxygen deficiency and Ru/Ti intermixing in the films. These findings provide insights into how quantum confinement tailors the metal-insulator transition and magnetic states in complex oxide heterostructures.

II. RESULTS AND DISCUSSION

A. Magnetic and magnetotransport characterizations

Epitaxial SRO films with thicknesses of 2, 3, 4, and 8 u.c. were grown on (001)-oriented and TiO_2-terminated $SrTiO_3$ (STO) substrates using pulsed-laser deposition (see Supplemental Material, experimental section [45]). The *in situ* reflective high-energy electron diffraction monitoring reveals that the first SRO layer has a thickness of 1.5 u.c., suggesting that the SRO films are SrO-layer terminated (see Fig. S1 [45]). With decreasing the film thickness, a FM metal to non-FM insulator transition occurs at the critical thickness of 3 u.c., as shown in the temperature (T)-dependent resistivity (ρ) and magnetization (M) measurements [see Figs. 1(b) and 1(c)]. The 8- and 4-u.c. films show a FM transition at ∼140 and ∼120 K, respectively, but no obvious magnetic transition can be seen in the $M(T)$ curves of 2- and 3-u.c. films, whereas, the anomalous Hall resistivity measurement [see Fig. 1(d)] clearly reveals a magnetic order in the 3-u.c. film and the magnetic transition temperature is ∼70 K. Compared to the 8- and 4-u.c. films (see Fig. S2 [45]), the anomalous Hall resistivity hysteresis loops of 3-u.c. film exhibit reversed

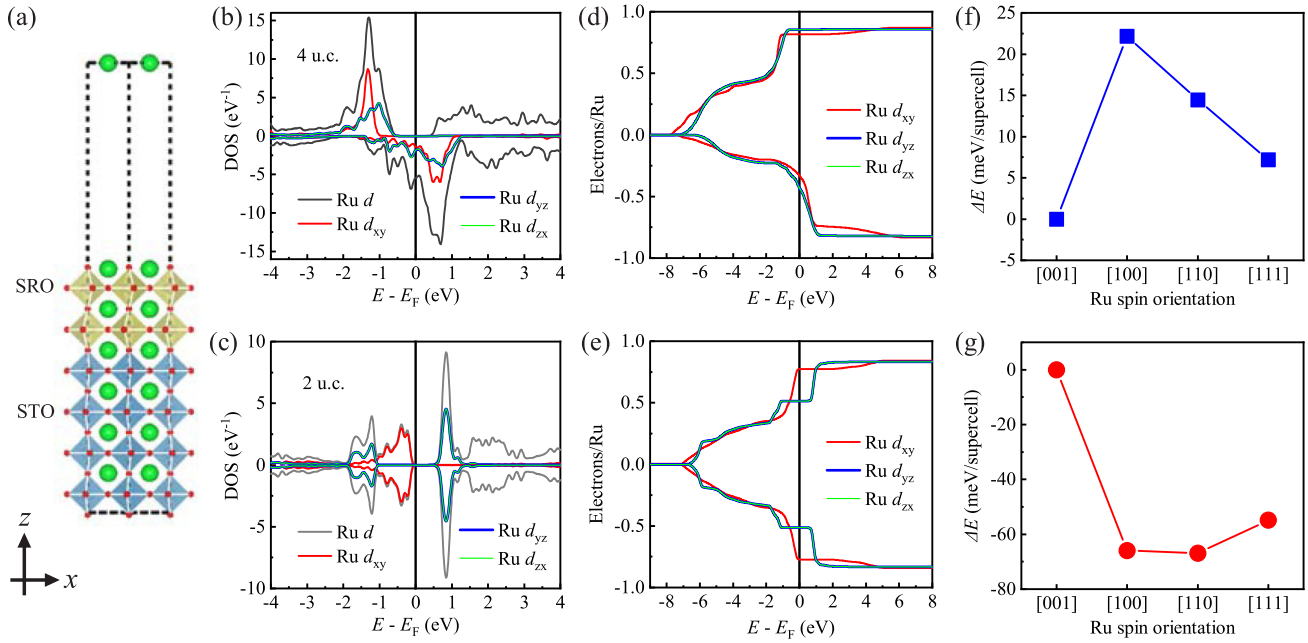

FIG. 2. First-principles calculations of ultrathin SRO films. (a) Schematic of the crystal structure of 2-u.c. SRO film used in the calculations. The dashed lines indicate the volume of a single supercell. Near Fermi-level density of states of Ru 4d orbitals of (b) 4-u.c. and (c) 2-u.c. SRO films calculated with $U = 3$ eV. Electron occupancies of Ru $4d_{xy}$ and $4d_{yz}/d_{zx}$ orbitals of (d) 4-u.c. and (e) 2-u.c. SRO films. Total energies with Ru spins along the [001], [100], [110], and [111] directions of (f) 4-u.c. and (g) 2-u.c. SRO films. Energy of the [001] state is used as the reference.

polarity, reduced coercivity, and much smaller saturation resistivity. These observations demonstrate that the 3-u.c. film has a very different magnetic state compared to the thicker films.

Then, we further study the magnetic property of the films by measuring the magnetic-field angle-dependent resistivity (MAR). MAR is a magnetotransport counterpart of the magnetocrystalline anisotropy energy and has been demonstrated as a powerful tool to study the magnetic anisotropy in oxide thin films [46–52]. In the measurement, the longitudinal resistivity is recorded with sweeping the magnetic field (H) in YZ and XY planes, respectively [as schematically shown in Fig. 1(a), bottom panel]. Figs. 1(e) and 1(f) are the MARs of 8-, 4-, 3-, and 2-u.c. SRO films. Detailed temperature dependence of the MAR is shown in Supplemental Material Figs. S3 and S4 [45]. The MARs of 8-u.c. film all have a twofold symmetry and agree with a well-defined perpendicular magnetic anisotropy. The MAR of H in the YZ plane arises from the spin-dependent electron scattering while the MAR of H in the XY plane is due to the normal anisotropic magnetoresistance (AMR) effect [53]. Similarly, the 4-u.c. film also has a dominant PMA, but with additional peaks at $90^\circ/270^\circ$ in the MAR with H in the XY plane. The MARs with H in the YZ plane of 3- and 2-u.c. films show a reversed polarity, and the MARs with H in the XY plane exhibit a nearly fourfold symmetry with resistivity minimum when H is in the fourfold [110] directions. The fourfold MAR could not arise from the normal AMR effect and should be attributed to the magnetocrystalline component of 3- and 2-u.c. films. Furthermore, the temperature-dependent MAR value at $\theta_Z = 90^\circ$ of 2-u.c. film [see Fig. 1(g)] indicates a transition around 70 K, in good coincidence with the anomalous Hall results. This observation suggests that the evolution in the MARs of 3- and 2-u.c. films originates from the magnetic order. Therefore, the combined MAR measurements in YZ and XY planes indicate an in-plane ⟨110⟩ magnetic anisotropy in the 3- and 2-u.c. SRO films. We then measured the $M(H)$ loops along the [001] and [110] directions of the 3-u.c. film (see Supplemental Material Fig. S5) which also demonstrate that the [110] direction is the magnetic easy axis. As the 3- and 2-u.c. SRO films are magnetic insulators with well-defined magnetic anisotropy but have negligible net moment, they can be inferred as an AFM state (this will be further confirmed theoretically later). Therefore, the magnetic and transport measurements demonstrate that the 8- and 4-u.c. SRO films are FM metal with PMA while the 3- and 2-u.c. films are AFM insulator with ⟨110⟩ magnetic anisotropy [as schematically shown in Fig. 1(a), top panel].

B. First-principles calculations

To understand the origin of the magnetic phase transition depending on thickness in the ultrathin SRO films, we perform density-functional theory calculations within the GGA plus Hubbard on-site Coulomb repulsion U (see Supplemental Material for details [45]). We built slabs with 2-, 3-, or 4-u.c. SRO layers capped on 4-u.c. STO and 20-Å vacuum for the calculations, where the SRO layer is SrO terminated, in accordance with the experimental results. Fig. 2(a) displays the schematic illustration of 2-u.c. SRO supercell used in the calculations. Thick SRO films grown on STO substrates usually have an $a^- b^+ c^-$ OOR pattern, but the OOR about the in-plane axes

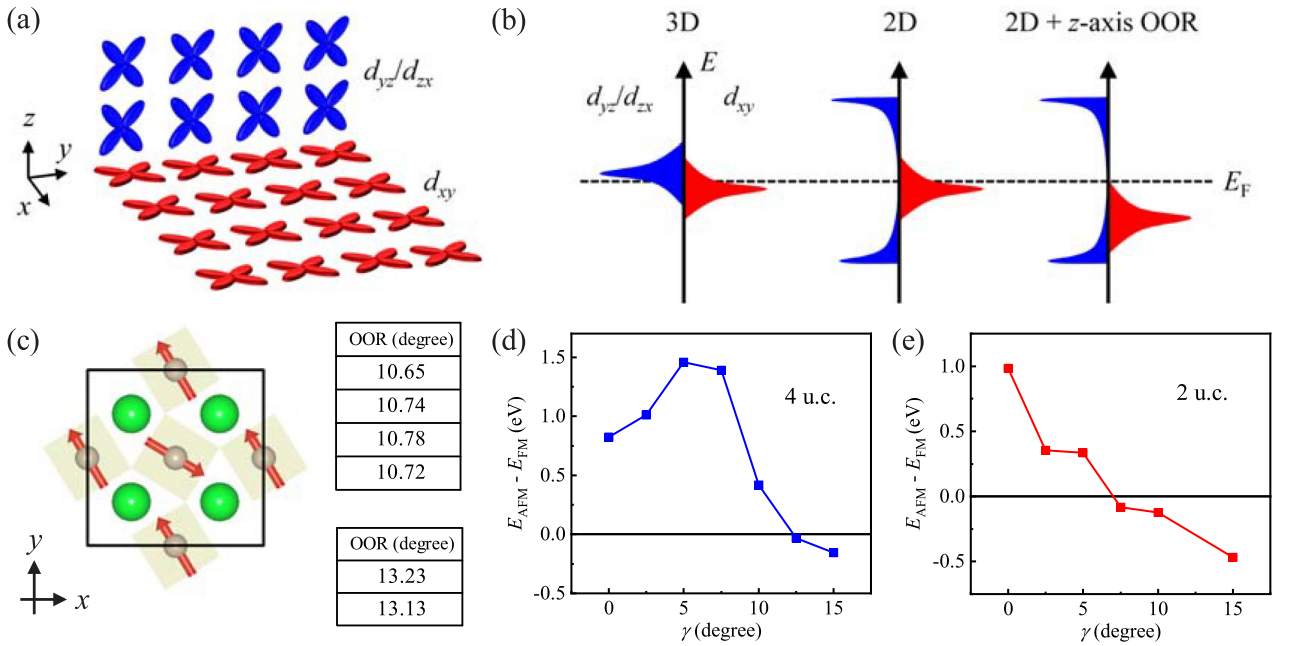

FIG. 3. Quantum confinement- and oxygen octahedral rotation-induced electronic reconstruction of ultrathin SRO films. (a) Schematic illustration of the connectivity of Ru d_{xy} and d_{yz}/d_{zx} orbitals. (b) Schematic demonstration of the reconstruction of Ru d_{xy} and d_{yz}/d_{zx} orbitals driven by reduced dimensionality and OOR along z axis. (c) Schematic of RuO_6 octahedral rotation along z axis and layer-dependent OOR angles of 4- and 2-u.c. SRO films. Energy difference between the FM and AFM states as a function of RuO_6 octahedral rotation angle γ in (d) 4-u.c. and (e) 2-u.c. SRO films.

will be greatly suppressed in the 2D limit [26,54]. Therefore, we only consider an $a^0a^0c^-$ rotation in this paper. In the ground-state energy calculations, we evaluate two possible alignments for the Ru spins, i.e., the FM and G-type AFM orders. Our DFT+U calculations unveil that the effective on-site Coulomb repulsion U makes a significant impact on the magnetic ground states that a larger U stabilizes the AFM state (see Fig. S6 [45]).

Figures 2(b) and 2(c) present the near Fermi-level partial density of states (PDOS) of Ru 4d orbitals of 4- and 2-u.c. SRO films with $U = 3$ eV. The 4-u.c. film is in FM half-metallic ground state, where the metallicity is mainly contributed by the spin minority channels of Ru d_{xy}, d_{yz}, and d_{zx} orbitals, whereas the 2-u.c. film has an AFM insulating ground state. With the film thickness down to 2 u.c., Ru d_{yz} and d_{zx} orbitals split into two subbands, consequently opening an energy gap, and Ru d_{xy} orbital resides in the gap with the Fermi level locating right at the top edge of the d_{xy} band. We then examine the electron occupancy of Ru 4d orbitals by integrating the DOS near the Fermi level [see Figs. 2(d) and 2(e)]. In SRO/STO heterostructures with itinerant FM, Ru^{4+} ions have a formal d^4 occupancy, where three electrons occupy the spin majority channels of Ru d_{xy} and d_{yz}/d_{zx} orbitals and the fourth electron occupies the spin minority channels. The SRO/STO interface removes the degeneracy between Ru d_{xy} and d_{yz}/d_{zx} orbitals that in the minority spin channels the d_{yz} and d_{zx} states are at lower energies compared to the d_{xy} state, causing a larger electron occupancy in the d_{yz}/d_{zx} orbital [6,40], as shown in the integrated PDOS of 4-u.c. SRO film [see Fig. 2(d)], whereas, for the 2-u.c. SRO film, due to the splitting of Ru d_{yz}/d_{zx} orbital and the reduced energy of Ru d_{xy} orbital, Ru 4d electrons will redistribute on the t_{2g} levels. As a result, in the 2-u.c. film the occupancy of Ru d_{xy} orbital increases, while the occupancy of Ru d_{yz}/d_{zx} orbital decreases and becomes smaller than that of Ru d_{xy} orbital [see Fig. 2(e)]. The reconstruction of Ru 4d orbitals will significantly modify the underlying spin-orbit interactions. Turning on the spin-orbit coupling to induce the magnetic anisotropy of the films [see Figs. 2(f) and 2(g)], we test four possible high-symmetry crystalline axes for Ru spins, i.e., [001], [100], [110], and [111]. The magnetic easy axis is along the [001] direction in the 4-u.c. film, but changes to the [110] direction in the 2-u.c. film. The 3-u.c. film is also an AFM insulator with [110] magnetic anisotropy (see Fig. S7 [45]). These calculation results in terms of ground states and magnetic anisotropies agree well with the magnetic and transport measurements. A previous DFT calculation also identified an in-plane magnetic easy axis in monolayer SRO [44].

The first-principles calculations reproduce the experimental discovery very well, highlighting the role of intrinsic dimensionality effect on the thickness-dependent MIT. In ultrathin SRO films, the magnetism and conductivity are mainly determined by Ru 4d t_{2g} orbitals [as schematically shown in Fig. 3(a)]. In the three-dimensional (3D) situation within a tight-binding model, both Ru d_{xy} and d_{yz}/d_{zx} orbitals form a 2D network, resulting in a 2D-type Van Hove singularity locating at the band center [6,36,55] [see Fig. 3(b), left panel]. This causes a high DOS at the Fermi level that is instable due to the enhanced effective Coulomb interaction and Hund's coupling [56]. The instability can be avoided by splitting Ru d_{xy} and d_{yz}/d_{zx} orbitals into spin majority and -minority bands, thus giving rise to FM metallic state as in the case of 4-u.c.

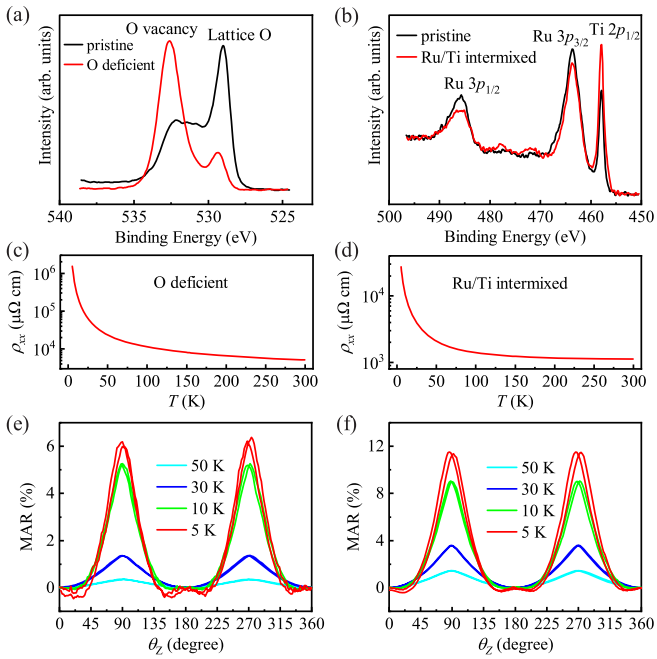

FIG. 4. Magnetic and transport measurements of defective SRO films. XPS spectra of (a) O-deficient and (b) Ru/Ti-intermixed 4-u.c. SRO films. Spectra of the pristine 4-u.c. film are shown for comparison. Temperature-dependent resistivities of (c) O-deficient and (d) Ru/Ti-intermixed 4-u.c. SRO films. MAR measurement of (e) O-deficient and (f) Ru/Ti-intermixed 4-u.c. SRO films. During the MAR measurement, 5-T magnetic field is rotated in the YZ plane. θ_Z is the angle between the field and z axis.

SRO film [Fig. 2(b)]. With reduced dimensionality, the 2D network of Ru d_{yz}/d_{zx} orbital turns into a one-dimensional (1D) strip, forming two separate singularities at each edge of the band [6,36,55] [see Fig. 3(b), middle panel]. This significantly reduces DOS of Ru d_{yz}/d_{zx} orbital at the Fermi level. But, the connectivity of Ru d_{xy} orbital has not changed and the orbital still contributes a high DOS at the Fermi level. Therefore, one may expect a metallic ground state of SRO films in the 2D limit as reported in many theoretical works [31,36].

However, our DFT+U calculations predict an AFM insulating state in the 3- and 2-u.c. SRO films. We find that the instability due to the high DOS of Ru d_{xy} orbital at the Fermi level can be removed by an enhanced OOR along the z axis. As shown in Fig. 3(c), the DFT+U calculation reveals that the OOR angle has increased from ∼10.7° in the 4-u.c. film to ∼13.2° in the 2-u.c. film. The OOR along the z axis will modify the hybridization between Ru d_{xy} and O $2p$ orbitals but has negligible effect on the bonding of Ru d_{yz}/d_{zx} orbital. It reduces the energy level of Ru d_{xy} orbital until the Fermi level reaches the top edge of the Ru d_{xy} band, which is exactly the case of 2-u.c. film [Fig. 2(c)]. Therefore, a zero DOS at the Fermi level can be constructed through the z-axis OOR [Fig. 3(b), right panel]. We then carried out a detailed investigation of how RuO_6 octahedral rotation angle γ affects the magnetic ground state. As shown in Figs. 3(d) and 3(e), at small γ the FM state is always more stable; only when γ is large enough, the AFM state is stabilized. And, experimentally, the prominent out-of-plane OOR in 3- and 2-u.c. SRO films can be confirmed in a recent publication [26]. It is precisely the interplay of QCE and OOR that gives rise to the AFM insulating state in the 3- and 2-u.c. films. And, it indicates that the FM metallic state in SRO monolayers could be obtained by capping/spacer layers such as $SrTiO_3$ and $BaTiO_3$ which suppress the OOR of RuO_6 octahedra [26,36–38]. In the G-type AFM phase, the Dzyaloshinskii-Moriya interaction arising from the z-axis OOR causes canting of Ru spin moment and concurrently a net moment along the fourfold ⟨110⟩ directions [as schematically shown in Fig. 3(c)]. Such spin alignment in 3- and 2-u.c. SRO films is reminiscent of the prototype pseudospin-canted AFM insulator Sr_2IrO_4 [57] that also displays a ⟨110⟩ magnetic anisotropy and a fourfold anisotropic magnetoresistance [46–48,58].

C. Exclusion of disorder factors

The good consistency between the experimental results and the first-principles calculations demonstrates that the MIT in ultrathin SRO films can be driven by the intrinsic dimensionality effect, specifically by the interplay of QCE and OOR. The appearance of the in-plane fourfold MAR in 2- and 3-u.c. films arises from the antiferromagnetic insulating phase, as confirmed by the first-principles calculations. The fourfold MAR begins to emerge in the 4-u.c. film, which may be caused by the thickness nonuniformity in this sample. But, the 8-u.c. film shows a pure twofold MAR, suggesting that there is not a dead layer in this sample. If the appearance of the antiferromagnetic insulating phase was due to substrate-to-film interactions such as interfacial strain/charge transfer, one would see the fourfold MAR in thick SRO films. Therefore, substrate-to-film interactions cannot be the driving force of the thickness-dependent MIT.

Furthermore, to exclude the extrinsic factor of structural/chemical disorders as another possible origin, we have fabricated two 4-u.c. SRO films as reference samples. An oxygen-deficient film was grown at reduced oxygen partial pressure of 5 Pa (see Fig. S8 [45] for structural information) and another film with Ru/Ti intermixing was prepared by substituting 25% Ru by Ti. X-ray photoelectron spectroscopy (XPS) measurement was performed to characterize the relative atomic ratios in SRO films. There is no signature of increased Ru vacancy with decreasing the film thickness (see Fig. S9 [45]). Though STO substrates contribute substantial O and Ti weights in the ultrathin films, the XPS spectra unambiguously confirm the significantly increased oxygen vacancy concentration [59] and Ru/Ti intermixing in the defective films [see Figs. 4(a) and 4(b)]. As shown in Figs. 4(c) and 4(d), both films display insulating transport behaviors which are driven by the defects, whereas the MARs of both films show similar evolutions with that of the pristine metallic 4-u.c. film [see Figs. 4(e) and 4(f)]. And, the PMA persists in the defective films while the IMA observed in the 3- and 2-u.c. films has not been reproduced. Therefore, though disorders can induce the MIT in SRO films, they cannot give rise to the AFM insulating state with ⟨110⟩ magnetic anisotropy.

III. CONCLUSIONS

In conclusion, our work has revealed how reduced dimensionality drives the transition from FM metal with perpendicular magnetic anisotropy to AFM insulator with in-plane magnetic anisotropy in itinerant ferromagnet SRO films in the 2D limit. The DFT calculations identified an orbital-selective quantum confinement and oxygen octahedral rotation in 3- and 2-u.c. SRO films. The resulting reconstruction of Ru 4*d* t_{2g} orbitals induces the antiferromagnetic insulating phase and reorients Ru magnetic easy axis along the ⟨110⟩ directions. These findings demonstrate that for 2D oxide materials, quantum confinement is a powerful tool to manipulate the electromagnetic properties. The spin reorientation from perpendicular to in-plane directions proposed in this work may act as a driving force of skyrmions in oxide films. And, our discovery provides strong evidence to one of the heavily disputed subjects in strongly correlated oxide heterostructures that reduced dimensionality alone can be the driving force of the dead-layer phenomenon.

ACKNOWLEDGMENTS

This work was supported by the National Natural Science Foundation of China (Grants No. 12004367 and No. 51627901), the National Key Research and Development Program of China (Grants No. 2016YFA0401004 and No. 2017YFA0402904), and Anhui Initiative in Quantum Information Technologies (Grant No. AHY100000).

[1] B. Huang, G. Clark, E. Navarro-Moratalla, D. R. Klein, R. Cheng, K. L. Seyler, D. Zhong, E. Schmidgall, M. A. McGuire, D. H. Cobden, W. Yao, D. Xiao, P. Jarillo-Herrero, and X. Xu, Nature (London) **546**, 270 (2017).

[2] C. Gong, L. Li, Z. Li, H. Ji, A. Stern, Y. Xia, T. Cao, W. Bao, C. Wang, and Y. Wang, Nature (London) **546**, 265 (2017).

[3] D. R. Klein, D. MacNeill, J. L. Lado, D. Soriano, E. Navarro-Moratalla, K. Watanabe, T. Taniguchi, S. Manni, P. Canfield, J. Fernandez-Rossier, and P. Jarillo-Herrero, Science **360**, 1218 (2018).

[4] A. Ohtomo and H. Y. Hwang, Nature (London) **427**, 423 (2004).

[5] H. Zhang, Y. Yun, X. Zhang, H. Zhang, Y. Ma, X. Yan, F. Wang, G. Li, R. Li, T. Khan, Y. Chen, W. Liu, F. Hu, B. Liu, B. Shen, W. Han, and J. Sun, Phys. Rev. Lett. **121**, 116803 (2018).

[6] M. Verissimo-Alves, P. Garcia-Fernandez, D. I. Bilc, P. Ghosez, and J. Junquera, Phys. Rev. Lett. **108**, 107003 (2012).

[7] N. Reyren, S. Thiel, A. D. Caviglia, L. F. Kourkoutis, G. Hammerl, C. Richter, C. W. Schneider, T. Kopp, A. S. Ruetschi, D. Jaccard, M. Gabay, D. A. Muller, J. M. Triscone, and J. Mannhart, Science **317**, 1196 (2007).

[8] Z. Chen, Z. Liu, Y. Sun, X. Chen, Y. Liu, H. Zhang, H. Li, M. Zhang, S. Hong, T. Ren, C. Zhang, H. Tian, Y. Zhou, J. Sun, and Y. Xie, Phys. Rev. Lett. **126**, 026802 (2021).

[9] K. Ueda, H. Tabata, and T. Kawai, Science **280**, 1064 (1998).

[10] K. S. Takahashi, M. Kawasaki, and Y. Tokura, Appl. Phys. Lett. **79**, 1324 (2001).

[11] L. Li, C. Richter, J. Mannhart, and R. C. Ashoori, Nat. Phys. **7**, 762 (2011).

[12] D. A. Dikin, M. Mehta, C. W. Bark, C. M. Folkman, C. B. Eom, and V. Chandrasekhar, Phys. Rev. Lett. **107**, 056802 (2011).

[13] A. J. Grutter, H. Yang, B. J. Kirby, M. R. Fitzsimmons, J. A. Aguiar, N. D. Browning, C. A. Jenkins, E. Arenholz, V. V. Mehta, U. S. Alaan, and Y. Suzuki, Phys. Rev. Lett. **111**, 087202 (2013).

[14] R. Scherwitzl, S. Gariglio, M. Gabay, P. Zubko, M. Gibert, and J. M. Triscone, Phys. Rev. Lett. **106**, 246403 (2011).

[15] M. Huijben, L. W. Martin, Y. H. Chu, M. B. Holcomb, P. Yu, G. Rijnders, D. H. A. Blank, and R. Ramesh, Phys. Rev. B **78**, 094413 (2008).

[16] D. Toyota, I. Ohkubo, H. Kumigashira, M. Oshima, T. Ohnishi, M. Lippmaa, M. Takizawa, A. Fujimori, K. Ono, M. Kawasaki, and H. Koinuma, Appl. Phys. Lett. **87**, 162508 (2005).

[17] H. Jeong, S. G. Jeong, A. Y. Mohamed, M. Lee, W.-s. Noh, Y. Kim, J.-S. Bae, W. S. Choi, and D.-Y. Cho, Appl. Phys. Lett. **115**, 092906 (2019).

[18] R. Yukawa, M. Kobayashi, T. Kanda, D. Shiga, K. Yoshimatsu, S. Ishibashi, M. Minohara, M. Kitamura, K. Horiba, A. F. Santander-Syro, and H. Kumigashira, Nat. Commun. **12**, 7070 (2021).

[19] G. Wang, Z. Wang, M. Meng, M. Saghayezhian, L. Chen, C. Chen, H. Guo, Y. Zhu, E. W. Plummer, and J. Zhang, Phys. Rev. B **100**, 155114 (2019).

[20] A. Biswas, K.-S. Kim, and Y. H. Jeong, J. Appl. Phys. **116**, 213704 (2014).

[21] A. Boris, Y. Matiks, E. Benckiser, A. Frano, P. Popovich, V. Hinkov, P. Wochner, M. Castro-Colin, E. Detemple, and V. K. Malik, Science **332**, 937 (2011).

[22] J. Liu, S. Okamoto, M. van Veenendaal, M. Kareev, B. Gray, P. Ryan, J. W. Freeland, and J. Chakhalian, Phys. Rev. B **83**, 161102(R) (2011).

[23] K. Yoshimatsu, T. Okabe, H. Kumigashira, S. Okamoto, S. Aizaki, A. Fujimori, and M. Oshima, Phys. Rev. Lett. **104**, 147601 (2010).

[24] P. D. King, H. I. Wei, Y. F. Nie, M. Uchida, C. Adamo, S. Zhu, X. He, I. Bozovic, D. G. Schlom, and K. M. Shen, Nat. Nanotechnol. **9**, 443 (2014).

[25] P. Schutz, D. Di Sante, L. Dudy, J. Gabel, M. Stubinger, M. Kamp, Y. Huang, M. Capone, M. A. Husanu, V. N. Strocov, G. Sangiovanni, M. Sing, and R. Claessen, Phys. Rev. Lett. **119**, 256404 (2017).

[26] X. Zhang, A. N. Penn, L. Wysocki, Z. Zhang, P. H. M. van Loosdrecht, L. Kornblum, J. M. LeBeau, I. Lindfors-Vrejoiu, and D. P. Kumah, APL Mater. **10**, 051107 (2022).

[27] L. F. Kourkoutis, J. H. Song, H. Y. Hwang, and D. A. Muller, Proc. Natl. Acad. Sci. USA **107**, 11682 (2010).

[28] Z. Liao, F. Li, P. Gao, L. Li, J. Guo, X. Pan, R. Jin, E. W. Plummer, and J. Zhang, Phys. Rev. B **92**, 125123 (2015).

[29] Z. Ali, Z. Wang, A. O'Hara, M. Saghayezhian, D. Shin, Y. Zhu, S. T. Pantelides, and J. Zhang, Phys. Rev. B **105**, 054429 (2022).

[30] G. Koster, L. Klein, W. Siemons, G. Rijnders, J. S. Dodge, C.-B. Eom, D. H. A. Blank, and M. R. Beasley, Rev. Mod. Phys. **84**, 253 (2012).
[31] Y. J. Chang, C. H. Kim, S. H. Phark, Y. S. Kim, J. Yu, and T. W. Noh, Phys. Rev. Lett. **103**, 057201 (2009).
[32] J. Xia, W. Siemons, G. Koster, M. R. Beasley, and A. Kapitulnik, Phys. Rev. B **79**, 140407(R) (2009).
[33] K. Ishigami, K. Yoshimatsu, D. Toyota, M. Takizawa, T. Yoshida, G. Shibata, T. Harano, Y. Takahashi, T. Kadono, V. K. Verma, V. R. Singh, Y. Takeda, T. Okane, Y. Saitoh, H. Yamagami, T. Koide, M. Oshima, H. Kumigashira, and A. Fujimori, Phys. Rev. B **92**, 064402 (2015).
[34] D. Toyota, I. Ohkubo, H. Kumigashira, M. Oshima, T. Ohnishi, M. Lippmaa, M. Kawasaki, and H. Koinuma, J. Appl. Phys. **99**, 08N505 (2006).
[35] X. Shen, X. Qiu, D. Su, S. Zhou, A. Li, and D. Wu, J. Appl. Phys. **117**, 015307 (2015).
[36] B. Sohn, J. R. Kim, C. H. Kim, S. Lee, S. Hahn, Y. Kim, S. Huh, D. Kim, Y. Kim, W. Kyung, M. Kim, M. Kim, T. W. Noh, and C. Kim, Nat. Commun. **12**, 6171 (2021).
[37] M. Ye, S. Hu, Y. Zhu, Y. Zhang, S. Ke, L. Xie, Y. Zhang, S. Hu, D. Zhang, Z. Luo, M. Gu, J. He, P. Zhang, W. Zhang, and L. Chen, Nano Lett. **21**, 144 (2021).
[38] H. Boschker, T. Harada, T. Asaba, R. Ashoori, A. V. Boris, H. Hilgenkamp, C. R. Hughes, M. E. Holtz, L. Li, D. A. Muller, H. Nair, P. Reith, X. Renshaw Wang, D. G. Schlom, A. Soukiassian, and J. Mannhart, Phys. Rev. X **9**, 011027 (2019).
[39] J. M. Rondinelli, N. M. Caffrey, S. Sanvito, and N. A. Spaldin, Phys. Rev. B **78**, 155107 (2008).
[40] P. Mahadevan, F. Aryasetiawan, A. Janotti, and T. Sasaki, Phys. Rev. B **80**, 035106 (2009).
[41] K. Gupta, B. Mandal, and P. Mahadevan, Phys. Rev. B **90**, 125109 (2014).
[42] C. Autieri, J. Phys.: Condens. Matter. **28**, 426004 (2016).
[43] S. G. Jeong, T. Min, S. Woo, J. Kim, Y. Q. Zhang, S. W. Cho, J. Son, Y. M. Kim, J. H. Han, S. Park, H. Y. Jeong, H. Ohta, S. Lee, T. W. Noh, J. Lee, and W. S. Choi, Phys. Rev. Lett. **124**, 026401 (2020).
[44] K. Samanta, M. Ležaić, M. Merte, F. Freimuth, S. Blügel, and Y. Mokrousov, J. Appl. Phys. **127**, 213904 (2020).
[45] See Supplemental Material at http://link.aps.org/supplemental/10.1103/PhysRevB.107.064418 for details on methods and additional data of structural characterizations, transport measurements, and first-principles calculations, which includes Refs. [60–68].
[46] H. Wang, C. Lu, J. Chen, Y. Liu, S. L. Yuan, S.-W. Cheong, S. Dong, and J.-M. Liu, Nat. Commun. **10**, 2280 (2019).
[47] C. Lu, B. Gao, H. Wang, W. Wang, S. Yuan, S. Dong, and J.-M. Liu, Adv. Funct. Mater. **28**, 1706589 (2018).
[48] H. Xu, H. Huang, Q. Wu, Z. Wang, Z. Cui, X. Zhai, J. Wang, Z. Fu, and Y. Lu, J. Mater. Sci. **55**, 8211 (2020).
[49] D. Tian, Z. Liu, S. Shen, Z. Li, Y. Zhou, H. Liu, H. Chen, and P. Yu, Proc. Natl. Acad. Sci. USA **118**, e2101946118 (2021).
[50] Z. Cui, A. J. Grutter, H. Zhou, H. Cao, Y. Dong, D. A. Gilbert, J. Wang, Y.-S. Liu, J. Ma, Z. Hu, J. Guo, J. Xia, B. J. Kirby, P. Shafer, E. Arenholz, H. Chen, X. Zhai, and Y. Lu, Sci. Adv. **6**, eaay0114 (2020).
[51] D. Yi, J. Liu, S. L. Hsu, L. Zhang, Y. Choi, J. W. Kim, Z. Chen, J. D. Clarkson, C. R. Serrao, E. Arenholz, P. J. Ryan, H. Xu, R. J. Birgeneau, and R. Ramesh, Proc. Natl. Acad. Sci. USA **113**, 6397 (2016).
[52] A. K. Jaiswal, D. Wang, V. Wollersen, R. Schneider, M. L. Tacon, and D. Fuchs, Adv. Mater. **34**, e2109163 (2022).
[53] E. D. Dahlberg, K. Riggs, and G. A. Prinz, J. Appl. Phys. **63**, 4270 (1988).
[54] W. Lu, P. Yang, W. D. Song, G. M. Chow, and J. S. Chen, Phys. Rev. B **88**, 214115 (2013).
[55] S. Kang, Y. Tseng, B. H. Kim, S. Yun, B. Sohn, B. Kim, D. McNally, E. Paris, C. H. Kim, C. Kim, T. W. Noh, S. Ishihara, T. Schmitt, and J. G. Park, Phys. Rev. B **99**, 045113 (2019).
[56] H. J. Lee, C. H. Kim, and A. Go, Phys. Rev. B **102**, 195115 (2020).
[57] B. J. Kim, H. Ohsumi, T. Komesu, S. Sakai, T. Morita, H. Takagi, and T. Arima, Science **323**, 1329 (2009).
[58] I. Fina, X. Marti, D. Yi, J. Liu, J. H. Chu, C. Rayan-Serrao, S. Suresha, A. B. Shick, J. Zelezny, T. Jungwirth, J. Fontcuberta, and R. Ramesh, Nat. Commun. **5**, 4671 (2014).
[59] S. A. Lee, S. Oh, J.-Y. Hwang, M. Choi, C. Youn, J. W. Kim, S. H. Chang, S. Woo, J.-S. Bae, S. Park, Y.-M. Kim, S. Lee, T. Choi, S. W. Kim, and W. S. Choi, Energy Environ. Sci. **10**, 924 (2017).
[60] G. Kresse and J. Furthmuller, Comput. Mater. Sci. **6**, 15 (1996).
[61] J. P. Perdew, K. Burke, and M. Ernzerhof, Phys. Rev. Lett. **77**, 3865 (1996).
[62] F. Wu, E. Kan, C. Tian, and M. H. Whangbo, Inorg. Chem. **49**, 7545 (2010).
[63] H. J. Koo, H. Xiang, C. Lee, and M. H. Whangbo, Inorg. Chem. **48**, 9051 (2009).
[64] L. Wang, Q. Feng, Y. Kim, R. Kim, K. H. Lee, S. D. Pollard, Y. J. Shin, H. Zhou, W. Peng, D. Lee, W. Meng, H. Yang, J. H. Han, M. Kim, Q. Lu, and T. W. Noh, Nat. Mater. **17**, 1087 (2018).
[65] J. Matsuno, N. Ogawa, K. Yasuda, F. Kagawa, W. Koshibae, N. Nagaosa, Y. Tokura, and M. Kawasaki, Sci. Adv. **2**, e1600304 (2016).
[66] Q. Qin, L. Liu, W. Lin, X. Shu, Q. Xie, Z. Lim, C. Li, S. He, G. M. Chow, and J. Chen, Adv. Mater. **31**, e1807008 (2019).
[67] D. Kan, T. Moriyama, K. Kobayashi, and Y. Shimakawa, Phys. Rev. B **98**, 180408(R) (2018).
[68] A. Gerber, Phys. Rev. B **98**, 214440 (2018).